Impact of Thermochemical Nonequilibrium Effects on the Supersonic Mode in Hypersonic Boundary Layers

Carleton P. Knisely* and Xiaolin Zhong†

University of California, Los Angeles, California, 90095, USA

The supersonic mode in hypersonic boundary layers has been shown to be associated with an unstable Mack's second mode synchronizing with the slow acoustic spectrum, causing the disturbance to travel upstream supersonically relative to the mean flow outside the boundary layer. The flow conditions leading to the supersonic mode have not been thoroughly and systematically investigated. As a result, it is unknown whether or not the supersonic mode can become the dominant boundary layer instability over the traditional second mode. This work uses thermochemical nonequilibrium Linear Stability Theory (LST) to obtain a more complete investigation of the supersonic mode using both nonequilibrium and perfect gas models. The mean flow is obtained from Direct Numerical Simulation (DNS) assuming both thermochemical nonequilibrium and frozen flow models. The purpose is to analyze the real gas effect on the supersonic mode at conditions typical of experimental conditions. The simulation is Mach 5 flow over a 1 mm nose radius axisymmetric cone 1 meter in length. The LST results indicate that vibrational nonequilibrium effects are stabilizing to the second and supersonic modes. The nonequilibrium effects in the mean flow, however, are not as critical. Overall, the LST results demonstrate the importance of accounting for nonequilibrium effects when studying the supersonic mode.

I. Introduction

The boundary layer transition location in hypersonic flow has long been known to be critical in the design of hypersonic vehicle.[1–3] Turbulent flow is associated with significantly higher skin drag and surface heating rates compared to laminar flow. Therefore, accurately predicting the onset of transition to turbulence allows for a more accurate specification of thermal protection system (TPS) thickness, reducing vehicle weight and enabling a larger payload.

The dominant hypersonic boundary layer transition mechanism in axisymmetric, zero angle-of-attack flows is Mack's second mode.[4] Physically, the second mode has been visualized as a trapped acoustic wave between the wall and the relative sonic line.[3,5] However, this description of the second mode assumes a neutral mode with large wave number, which is not particularly realistic. Although the physical phenomena differs from this mathematical definition, it is still instructive to visualize the behavior of the second mode with acoustic-like behavior in mind for comparison to 2D LST and DNS contours as well as experimental imaging techniques.

The local relative Mach number provides insight into the boundary layer disturbance structure. It is expressed as

$$\overline{M}(y) = \frac{\overline{u}(y) - c_r}{\overline{a}(y)} \tag{1}$$

where $\overline{u}(y)$ is the local mean flow velocity tangential to the wall, $c_r = \omega/\sqrt{\beta_r^2 + \alpha_r^2}$ is the real component of the disturbance propagation speed with ω the circular frequency, β_r the spanwise wavenumber, and α_r the real component of the streamwise wave number, and $\overline{a}(y)$ is the local mean flow speed of sound. The region of acoustic-like modulation between the wall and the relative sonic line is characterized by a region in which $\overline{M}(y) < -1$, indicating the disturbance is traveling downstream supersonically w.r.t. the local flow. Outside

*Graduate Student, Mechanical and Aerospace Engineering, carleton.knisely@gmail.com, AIAA Student Member.

†Professor, Mechanical and Aerospace Engineering, xiaolin@seas.ucla.edu, AIAA Associate Fellow.

of the sonic line y_a where $\overline{M}(y_a) = -1$, the disturbance travels subsonically w.r.t. the local flow. At the critical layer y_c where $\overline{M}(y_c) = 0$ the disturbance phase speed is equal to the local mean flow velocity and the "rope-like" structures are observed.[6–10]

The supersonic mode can be visualized using similar reasoning, however it is characterized by a second relative sonic line at $\overline{M} = 1$. Outside of this second relative sonic line the disturbance is traveling upstream supersonically w.r.t. the local flow, resulting in the decaying Mach-wave like structures shown in the schematic in Fig. 1. This wave pattern is analogous to the Mach wave from traditional compressible flow theory and is indeed approximated by $\mu \approx \arcsin(1/\overline{M})$. The relation for the angle is not exact due to the imaginary component of the wavenumber α.

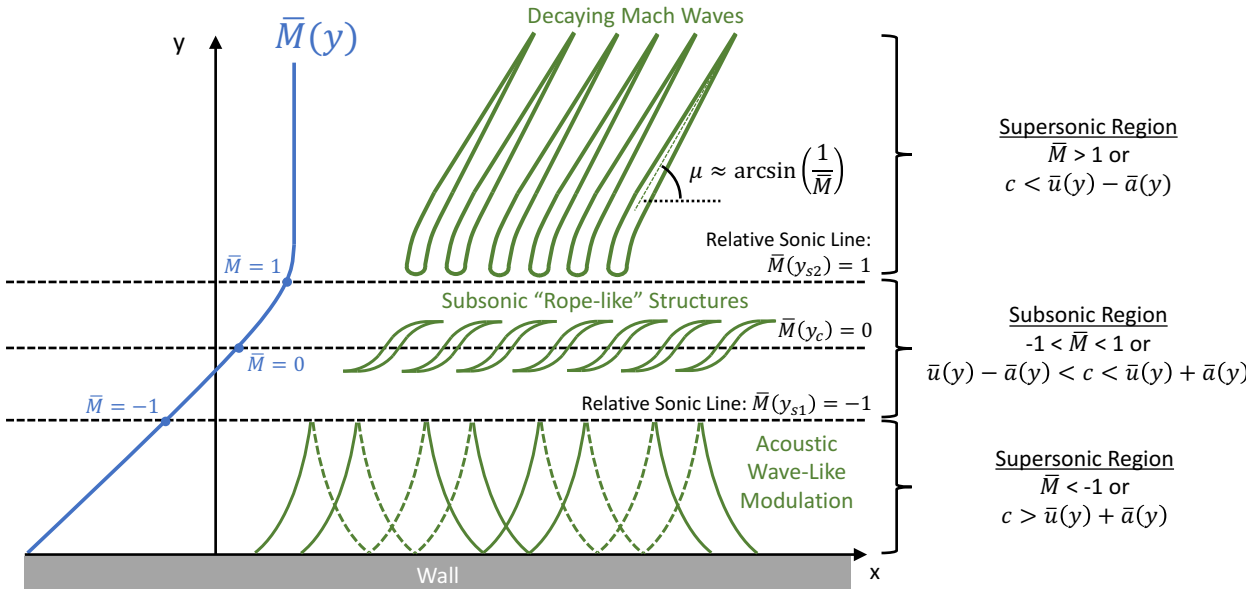

Figure 1. Visualization of supersonic mode (not strict mathematical model).

Although the supersonic mode has been known to exist since the mid-1980's by Mack[11,12] and Reshotko,[1] the general consensus was that the supersonic mode had a significantly smaller peak growth rate than the traditional second mode, and therefore was not a serious factor in transition to turbulence. Since then, only a few studies have been performed with the supersonic mode as the direct focus of the investigation,[13,14] although many researchers have encountered it in other contexts.[15–21] A recent renewal of interest in the supersonic mode was sparked by the thermal nonequilibrium LST analysis by Bitter and Shepherd in 2015.[22] The following year, Chuvakhov and Fedorov[23] largely confirmed Bitter and Shepherd's[22] findings through perfect gas LST analysis as well as unsteady DNS analysis on a flat plate, although they used different free stream conditions. In 2017, Edwards and Tumin[24] incorporated additional source terms in their mean flow equations accounting for kinetic fluctuations in the flow, but used a perfect gas stability solver. Edwards and Tumin suggested that these kinetic fluctuations may generate a discrete mode in vicinity of the neutral point. Depending on the flow parameters, the excited mode can become supersonic far downstream in vicinity of the upper neutral branch curve. In addition, in 2018 Knisely and Zhong[25] performed thermochemical nonequilibrium LST and DNS studies using similar hot wall flow conditions on a 5-degree half-angle blunt cone and confirmed the existence of the supersonic mode, although it was quite weak and was due to the interaction of mode S, mode F1, and the slow acoustic continuous spectrum. This phenomenon may be attributed to the real gas effect and may have been overlooked in previous simulations assuming chemical equilibrium. Later in 2018, Knisely and Zhong[26] and Mortensen[27] showed the supersonic mode can have a higher growth rate than the traditional second mode under certain conditions, demonstrating the importance of investigating this mechanism.

Overall, the impact of nonequilibrium chemistry and vibrational effects on the supersonic mode are not fully understood. With respect to the second mode, Linear Stability Theory (LST) and Parabolized Stability Equations (PSE) for nonequilibrium gases have been widely used.[28–32] Overall, it has been determined that dissociation of air species is stabilizing to the first mode, but destabilizing to the second mode. Additionally,

it was determined that thermal nonequilibrium has a slight destabilizing effect on the first mode, and a slight stabilizing effect on the second mode. This study performs an investigation of the impact of thermochemical nonequilibrium on the supersonic mode. Mean flow from DNS is obtained using both thermochemical nonequilibrium and frozen flow models. Additionally, the impact of a perfect gas vs. a thermochemical nonequilibrium LST solver is examined.

II. Simulation Conditions

The flow conditions for this study are summarized in Table 1 and are intended to be similar to those used by Bitter and Shepherd.[22] These flow conditions were also used by Knisely and Zhong in 2017.[33] Case 1 uses a thermochemical nonequilibrium model, while Case 2 assumes frozen flow. The geometry is a 5 degree half-angle axisymmetric blunt cone 1 meter in length with a nose radius of 1 mm. The DNS simulations used 256 points in the wall-normal direction and roughly 5 points per millimeter on the surface of the cone in the streamwise direction. In the azimuthal direction, four points are used. LST simulations interpolated the DNS meanflow onto the LST grid defined by the stretching methods discussed in the following sections.

Table 1. Freestream flow conditions for DNS simulations.

Parameter	Value	Parameter	Value
M_∞	5	$H_{0,\infty}$	9.17 MJ/kg
ρ_∞	2.322 E-2 kg/m^3	p_∞	10 kPa
T_∞	1500 K	U_∞	3882.42 m/s
c_{N_2}	0.78	c_{O_2}	0.22

As will be explained in the following sections, the DNS code used in this study utilizes a shock-fitting method. Thus, the parameters in Table 1 are the free stream conditions upstream of the shock formed over the body.

III. Governing Equations and Gas Model

The governing equations for the DNS and LST codes are those developed by Mortensen and Zhong,[34–39] which are formulated for thermochemical nonequilibrium assuming a two-temperature model. Their formulation is highlighted here for clarity. The rotational mode is assumed to be fully excited with up to eleven non-ionizing species with finite-rate chemistry. Two-temperatures are used to represent translation-rotation energy and vibration energy. There are two species models: an eleven-species model (N_2, O_2, NO, C_3, CO_2, C_2, CO, CN, N, O, C) used for ablation studies and a five-species model (N_2, O_2, NO, N, and O) used to simulate air. The five species model is used here. The Navier-Stokes equations in conservative form consist of five species mass conservation equations, three momentum conservation equations, the total energy equation, and the vibration energy equation. The governing equations in vector form are written as

$$\frac{\partial U}{\partial t} + \frac{\partial F_j}{\partial x_j} + \frac{\partial G_j}{\partial x_j} = W \tag{2}$$

where U is the state vector of conserved quantities, W is the source terms, and F_j and G_j are the inviscid and viscous flux vectors, respectively. For further details of the governing equations and thermochemical model, see the work of Knisely and Zhong[25,33] and Mortensen.[39]

IV. Numerical Methods

A. DNS

The thermochemical nonequilibrium code developed by Mortensen and Zhong[34–39] utilizes a high-order shock-fitting method extended from a perfect gas flow version by Zhong[40] to compute the flow field between the shock and the body. The numerical method is summarized here for clarity. For shock-fitting computations

the shock location is not known *a priori*, so its position is solved along with the flow field. Since the shock position is not stationary, the grid used to compute the flow field is a function of time. The Navier-Stokes equations are transformed into computational space

$$\frac{1}{J}\frac{\partial U}{\partial \tau}+\frac{\partial E'}{\partial \xi}+\frac{\partial F'}{\partial \eta}++\frac{\partial G'}{\partial \zeta}+\frac{\partial E'_v}{\partial \xi}+\frac{\partial F'_v}{\partial \eta}++\frac{\partial G'_v}{\partial \zeta}+U\frac{\partial (1/J)}{\partial \tau}=\frac{W}{J} \tag{3}$$

where J is the Jacobian of the coordinate transformation. Further details of this transformation can be found in Knisely and Zhong[25,33] and Mortensen.[39] A seven point stencil is used to discretize the spatial derivatives

$$\frac{\partial f_i}{\partial x}=\frac{1}{hb_i}\sum_{k=-3}^{3}\alpha_{i+k}f_{i+k}-\frac{\alpha}{6!b_i}h^5\left(\frac{\partial f^6}{\partial^6 x}\right) \tag{4}$$

where h is the step size, $\alpha<0$ is a fifth order upwind explicit scheme, and $\alpha=0$ reduces to a sixth order central scheme. Here the inviscid terms use $\alpha=-6$ which yields a low dissipation fifth order upwinded difference and the viscous terms are discretized using $\alpha=0$. The derivatives in the transverse direction, if required, are treated with Fourier collocation. To compute second derivatives, the first order derivative operator is applied twice. Flux splitting is used for the inviscid flux terms with the eigenvalues of Λ for thermochemical nonequilibrium derived by Liu and Vinokur.[41]

Conditions behind the shock are calculated from Rankine-Hugoniot relations. In the free stream, the flow is assumed to be in thermal equilibrium and the chemical composition of the flow is frozen. The shock is assumed to be infinitely thin which means that the flow has no time to relax as it crosses the shock as relaxation rates are finite. This leads to the chemical composition remaining constant across the shock, as well as the vibration temperature. Since neither process has any time to relax across the shock, the relaxation zone is entirely downstream of the shock. A complete derivation of thermochemical nonequilibrium shock fitting can be found in Prakash et al.[42] A low storage 1st-order Runge-Kutta method from Williamson[43] is used to advance the solution in time.

B. LST

The perfect gas LST solver is based on Malik's[44] and has been verified and utilized extensively.[45–47] The thermochemical nonequilbrium linear stability analysis used here has been derived and verified by Knisely and Zhong.[33] The LST equations are derived from the governing equations (either perfect gas or thermochemical nonequilbrium) in which the perturbations are assumed to be in the form of a normal mode described by $q'=\hat{q}(y)\exp\left[i\left(\alpha x+\beta z-\omega t\right)\right]$, where ω is the circular frequency of the disturbance and α and β are the wavenumbers. For comparison to direct numerical simulation the spatial stability approach is used i.e. α is complex which results in the dispersion relation $\alpha=\Omega(\omega,\beta)$. Substituting in the normal mode form for the perturbation reduces the problem to a coupled set of ordinary differential equations

$$\left(\mathbf{A}\frac{d^2}{dy^2}+\mathbf{B}\frac{d}{dy}+\mathbf{C}\right)\vec{\phi}=\vec{0}. \tag{5}$$

where $\vec{\phi}$ is the disturbance eigenvectors and $\mathbf{A}$, $\mathbf{B}$ and $\mathbf{C}$ are complex square matrices. This is now a boundary value problem where the derivative operators can be discretized and the equations solved numerically.

With the grid defined, Eq. 5 can be transformed into computational space and a numerical representation of the derivatives can be given. The perfect gas LST solver uses a multi-domain spectral collocation method, whereas the thermochemical nonequilibrium LST solver is discretized by taking derivatives of Lagrange polynomials in physical space. Here, a five-point stencil is used, resulting in a 4th order method similar to the one used in the perfect gas LST solver.

After discretization, nonlinearities exist in α so the global method suggested by Malik[44] is used to compute the eigenvalue spectrum with $\alpha^2=0$. This method computes the eigenvalues from a generalized eigenvalue problem $\tilde{A}\vec{\phi}=\alpha\tilde{B}\vec{\phi}$ where the LAPACK[48] subroutine ZGGEV is used here for solution. From the eigenvalue spectrum an initial guess can be obtained for the local method which results in $\overline{A}\vec{\phi}=\overline{B}$ and the eigenvalue is found iteratively without dropping the α^2 terms. The LAPACK subroutine ZGESV is used to solve the local problem. It is also possible to avoid the computationally intensive global method and obtain an initial guess for α from a nearby streamwise location or a DNS simulation assuming the unsteady DNS results are available.

The boundary conditions are required for the freestream and the wall. The wall boundary conditions are pressure extrapolation, no slip, and zero temperature perturbation, although more complex surface boundary conditions can be used for ablation studies.[35,39] In the freestream, the shock boundary conditions developed by Knisely and Zhong[33] were used for the thermochemical nonequilibrium LST solver, and Dirichlet (zero) boundary conditions were used for the perfect gas LST solver. It has been shown that the shock free stream boundary conditions are virtually indistinguishable from the Dirichlet when the computational domain is large.[33]

V. Steady Flow Field Solution

The steady DNS temperature and pressure contours for both Case 1 and Case 2 are shown in Fig. 2. There is a very clear disagreement in temperature between the nonequilibrium gas and frozen flow models (Fig. 2a), although the discrepancy between the pressure contour (Fig. 2b) is not as severe. Additionally, Case 1 (Noneq. model) has a slightly smaller shock height than Case 2 (Frozen Gas).

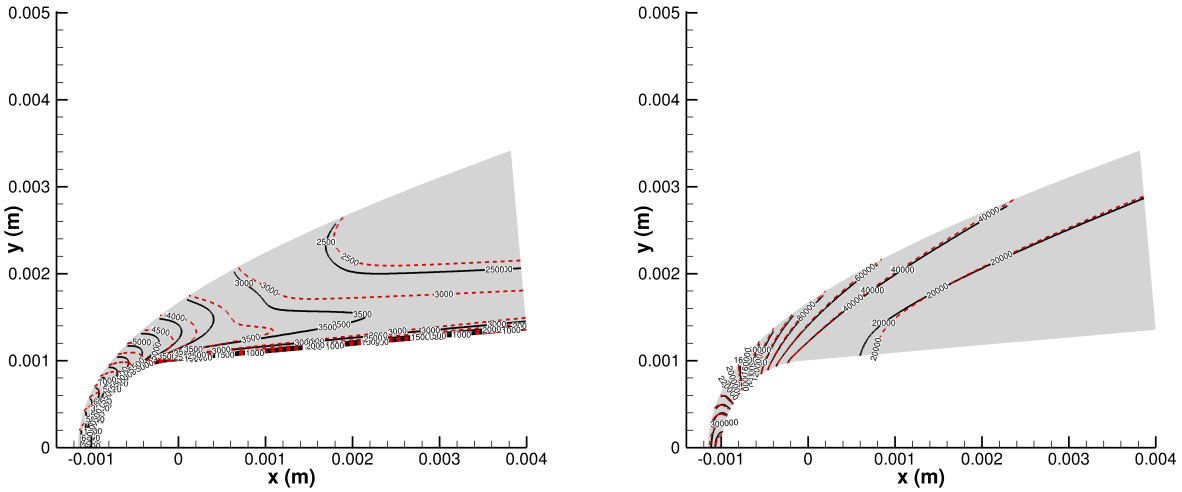

(a) (b)

Figure 2. Comparison of steady flow field contours in nose region. ——— Case 1 (Noneq. Model). - - - - - Case 2 (Frozen Gas Model). (a) Temperature, T (K). (b) Pressure, p (Pa).

Farther downstream, the difference between the nonequilibrium model and perfect gas flows diminish in the free stream, however there is still some difference within the boundary layer. Fig. 3 compares mean flow variables as a function of the wall-normal coordinate, y, with the axis limits modified to highlight the boundary layer region. The velocity and temperature of the perfect gas case differ slightly from the nonequilibrium case (Fig. 3a), particularly the peak temperature in the boundary layer, where there is approximately a 100 K difference between the models. Additionally, in the perfect gas model the vibration temperature is assumed to be zero, and is not included for comparison. The density of the flow follows similar trends (Fig. 3b), with the perfect gas model deviating slightly from the nonequilibrium gas model in the boundary layer. These seemingly small differences may have a significant impact on the stability of the flow.

VI. LST Results

The free stream values used in nondimensionalizing the results for Case 2 were the same as those for Case 1. In order to assess the impact of thermochemical nonequilibrium, the LST analysis of Case 1 was reproduced with a perfect gas LST solver, i.e. a perfect gas LST code was used to analyze the stability of the mean flow obtained from the nonequilibrium DNS. The perfect gas solver is based on Malik's multi-domain spectral method[44] and has been verified extensively.[45] Additionally, the perfect gas stability solver was used

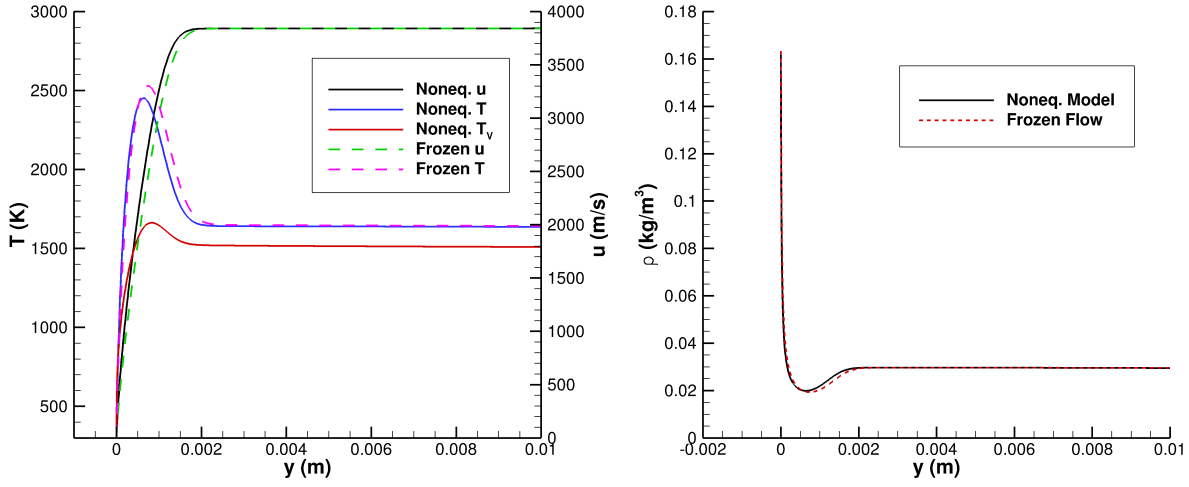

(a) (b)

Figure 3. Case 1 (Noneq. Model) and Case 2 (Frozen Gas) mean flow boundary layer profiles at $s = 0.4$ m. (a) u, T, and T_V. (b) Density ρ. u denotes the component of velocity tangential to the surface of the cone. y is the wall normal distance.

to analyze the stability of the mean flow obtained from the frozen flow DNS in Case 2. The phase speed and growth rate for a frequency of $f = 700$ kHz are shown in Fig. 4. It is apparent from the phase speeds in Fig. 4a that for mode F1+, the perfect gas LST using nonequilibrium mean flow and the perfect gas LST using frozen mean flow both agree with the fully nonequilibrium mode F1+. That is, it appears that the phase speed of mode F1+ is not impacted largely by nonequilibrium effects. Lastly, there appears to be only a small difference in phase speed between the perfect gas LST with nonequilbrium mean flow and with frozen mean flow. Using frozen flow compared to nonequilibrium mean flow with the perfect gas LST solver did not affect the phase speed significantly for both mode F1+ and mode S.

The growth rates in Fig. 4b, on the other hand, show significant differences depending on the LST gas model as well as the mean flow model. Regardless of the mean flow, the perfect gas LST predicts a significantly higher peak growth rate. Accordingly, this causes the supersonic mode "kink" in the perfect gas solver to have a higher magnitude than the nonequilibrium LST solver. The perfect gas solver having a larger magnitude growth rate than nonequilibrium is expected, as it is known that vibrational nonequilibrium effects are damping to the second mode. However, chemical nonequilibrium is known to be slightly destabilizing to the second mode. As mentioned by Knisely and Zhong[33] and Bitter and Shepherd,[22] the chemical effects in Case 1 are relatively weak, whereas the vibrational nonequilibrium is significant. Therefore, the perfect gas LST predicting a larger growth rate than the nonequilibrium LST is due to the vibrational energy mode absorbing some of the disturbance energy. This result suggests that the supersonic mode is affected by nonequilibrium effects in a similar manner as the traditional second mode.

Lastly, in Fig. 4b the maximum growth rate of the perfect gas LST with frozen mean flow is slightly lower in amplitude and occurs slightly upstream of the perfect gas LST with nonequilibrium mean flow. However, this difference is minimal and suggests the mean flow nonequilibrium effects are not as significant as they are in LST. This one case is far from sufficient to reach this conclusion, however, and the impact of nonequilibrium effects in the mean flow must be examined at higher enthalpy conditions.

Although the supersonic mode is visible with the perfect gas LST solver in Fig. 4, the new discrete mode F1- was not able to be resolved. This raises the question of the perfect gas LST solver's ability to capture the oscillatory eigenfunctions of supersonic modes. First, however, the comparison between the subsonic mode F1+ is compared between the nonequilibrium LST and the perfect gas LST with both nonequilibrium and frozen mean flow (Fig. 5). From Fig. 5a, it is clear that the nonequilibrium model has little effect on the shape of the pressure eigenfunction. The temperature eigenfunction in Fig. 5b, however, shows that the nonequilibrium LST solver produces a qualitatively similar shape, although the local maxima are of different

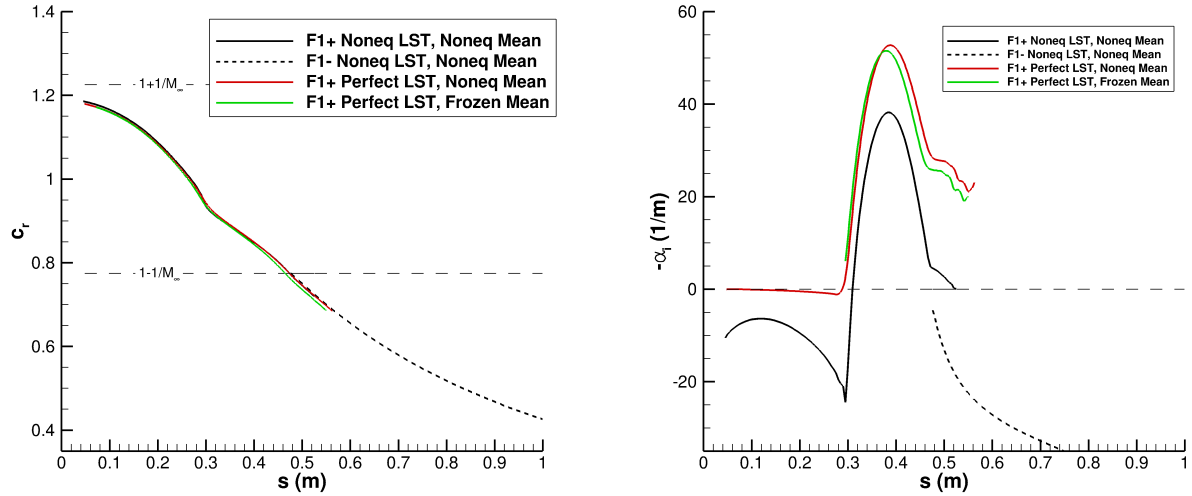

(a) (b)

Figure 4. LST phase speed and growth rate for Mode F1 at $f = 700$ MHz. (a) Phase Speed. (b) Growth Rate.

amplitudes than the perfect gas LST. These maxima are known to occur in regions where nonequilibrium activity occurs; therefore the difference in temperature eigenfunctions between the solvers is not surprising. There appears to be very little variation between the perfect gas LST using nonequilibrium mean flow vs. frozen mean flow in temperature eigenfunction, however.

The eigenvalues for the subsonic unstable mode F1+ are included in Table 2. The imaginary component of the wavenumber is the most differing parameter between the methods, with the fully nonequilibrium case showing the lowest value, followed by the perfect gas LST solver using frozen mean flow. The real component of the wavenumber does not vary as significantly, with the fully nonequilibrium case and the perfect gas LST solver using nonequilibrium mean flow showing nearly the same value. However, the perfect gas LST solver using frozen mean flow shows a slightly higher α_r, translating into a slightly lower phase speed. These trends in wavenumber were also visible in the phase speed and growth rate plots in Fig 4.

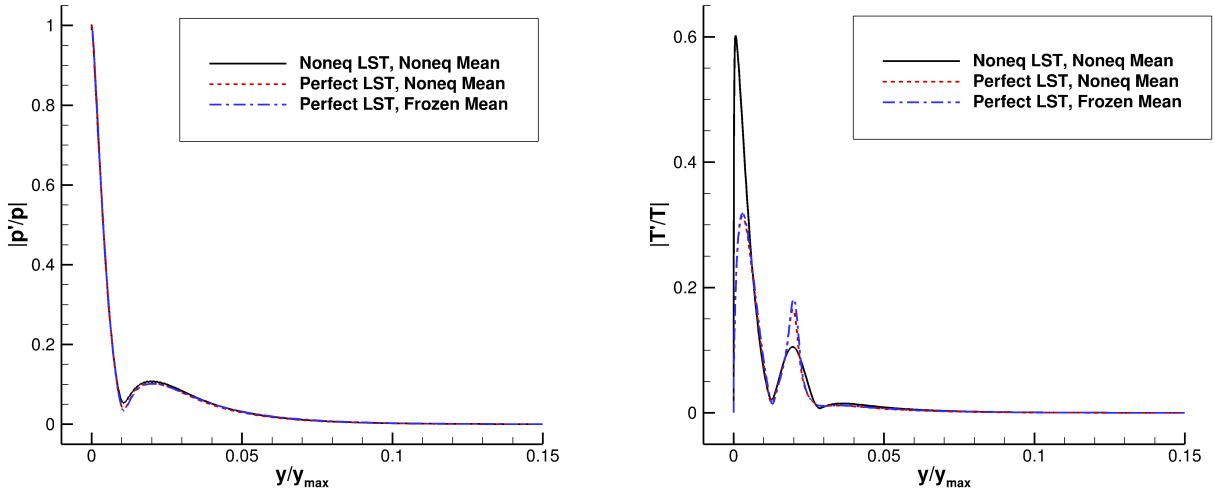

(a) (b)

Figure 5. Case 2 eigenfunctions normalized by local mean flow value for unstable second mode at $f = 700$ kHz, $s = 0.4224$ m. (a) Pressure. (b) Temperature.

The eigenvectors and eigenvalues of the supersonic mode at $s = 0.50$ m for $f = 700$ kHz are examined

Table 2. Eigenvalues for Case 2 subsonic unstable mode F1+ at $f = 700$ kHz, $s = 0.4224$ m.

LST Gas Model	Mean Flow Gas Model	α_r (1/m)	$-\alpha_i$ (1/m)
Noneq.	Noneq.	1366.12	30.73
Perfect	Noneq.	1367.00	47.25
Perfect	Frozen	1378.70	42.68

in Fig. 6 and Table 3, respectively. From the pressure eigenfunction in Fig. 6a, it is clear that the perfect gas LST solver does not display the amplification of the disturbance into the free stream as prominently as the nonequilibrium LST solver. That is, the amplitude of the pressure eigenfunction of the perfect gas LST, regardless of mean flow, decays to zero more rapidly outside the boundary layer than the nonequilibrium solver. Again, however, the perfect gas LST solver does not appear to be as dependent on the mean flow gas model. The perfect gas LST solver with nonequilibrium mean flow and frozen mean flow are virtually indistinguishable. The temperature eigenfunction in Fig. 6b shows similar trends. The perfect gas LST shows the amplitude of the temperature eigenfunction decaying to zero more rapidly than the nonequilibrium LST solver. Similar to the subsonic mode in Fig. 5b, the local maxima in the temperature eigenfunction are of different amplitude for the nonequilibrium LST solver than for the perfect gas solver.

The imaginary component of the wavenumber for the supersonic mode (Table 3) is again the most differing parameter between the methods, with the fully nonequilibrium case showing the lowest value, followed by the perfect LST solver using frozen mean flow. However, the difference in α_i is significantly greater for the supersonic mode than for the subsonic mode. Similar to the subsonic mode, however, the real component of the wavenumber does not vary as significantly, with the fully nonequilibrium case and the perfect gas LST solver using nonequilibrium mean flow showing nearly the same value. However, the perfect gas LST solver using frozen mean flow shows a slightly higher α_r, translating into a slightly lower phase speed. These trends in wavenumber were also visible in the phase speed and growth rate plots in Fig 4. Because α_r, and by extension the phase speed, of the supersonic mode obtained from the perfect gas LST solver agree reasonably with the nonequilibrium solver, it is possible that the perfect gas LST solver can be used to determine the relative location of the supersonic mode. However, because the perfect gas and the nonequilibrium gas LST solvers show wildly different values for α_i, it is inadvisable to use the perfect gas LST solver to predict supersonic mode growth rates.

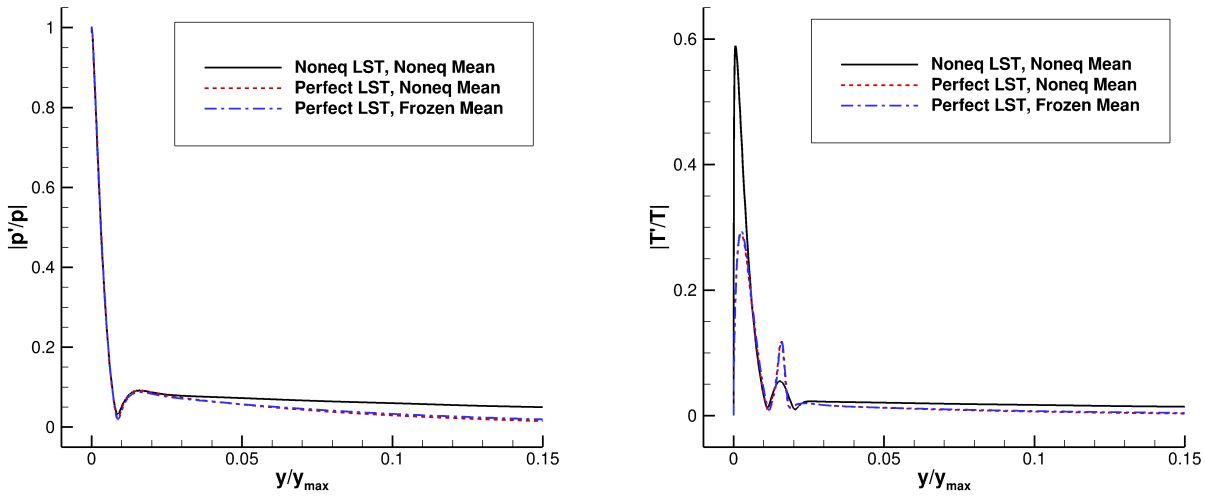

(a) (b)

Figure 6. Eigenfunctions normalized by local mean flow value for unstable supersonic mode at $f = 700$ kHz, $s = 0.50$ m. (a) Pressure. (b) Temperature.

Table 3. Eigenvalues for supersonic unstable mode F1+ at $f = 700$ kHz, $s = 0.50$ m.

LST Gas Model	Mean Flow Gas Model	α_r (1/m)	$-\alpha_i$ (1/m)
Noneq.	Noneq.	1520.71	2.623
Perfect	Noneq.	1521.40	27.31
Perfect	Frozen	1542.40	24.64

VII. Summary and Conclusion

There has been a resurgence of interest in studying the supersonic mode due to its presence and large amplification in some unexpected flow conditions.[24,26,27] However, the impact of thermochemical nonequilibrium effects on the stability of the supersonic mode is not fully understood. This study used Direct Numerical Simulation (DNS) with both thermochemical nonequilibrium and frozen flow models as mean flow inputs to Linear Stability Theory (LST) solvers. Both perfect gas and thermochemical nonequilbrium stability models were used to evaluate the impact of thermochemical nonequilbrium on the stability of the supersonic mode.

Overall, the supersonic mode appears to be stabilized and destabilized in a similar fashion as the second mode. Specifically, it was shown here that vibrational nonequilibrium is stabilizing to the supersonic mode. This result is expected as the supersonic mode is simply a special case of the second mode when the wave speed is slow enough such that the disturbance travels upstream supersonically with respect to the local mean flow. However, the more rapid decay of the eigenfunctions in the perfect gas LST solver indicates that it may not always be suitable for use in studying the supersonic mode. Furthermore, because the supersonic stable mode F1- was not able to be resolved with the perfect gas LST, it suggests that traditional LST solvers that do not account for nonequilibrium effects or oscillatory behavior in the free stream may provide inaccurate results when studying the supersonic mode. Although the location of the supersonic mode may be reasonably predicted by perfect gas LST, the amplitude is not as reliable and results should be used with caution.

Acknowledgments

This research was supported by the U.S. Air Force Office of Scientific Research (AFOSR) through the National Defense Science & Engineering Graduate Fellowship (NDSEG) Program. This research was also partially supported by the AFOSR, USAF, under AFOSR Grant #FA9550-15-1-0268, monitored by Dr. Ivett Leyva, and by Office of Naval Research (ONR) Grant #N00014-17-1-2343, monitored by Dr. Knox Millsaps previously and by Dr. Eric Marineau presently. Primary computational resources were provided by the AFOSR with additional computational resources provided by Extreme Science and Engineering Discovery Environment (XSEDE) through Texas Advanced Computing Center (TACC) and San Diego Supercomputer Center (SDSC) under grant number TG-ASC090076, supported in part by the National Science Foundation. The views and conclusions contained herein are those of the authors and should not be interpreted as necessarily representing the official policies or endorsements, either expressed or implied, of the U.S. Air Force Office of Scientific Research, Office of Naval Research, or the U.S. Government.

References

[1]Reshotko, E., "Hypersonic Stability and Transition," *Hypersonic flows for reentry problems*, Vol. 1, No. A93-42576 17-02, 1991, pp. 18–34.

[2]Zhong, X. and Wang, X., "Direct Numerical Simulation on the Receptivity, Instability, and Transition of Hypersonic Boundary Layers," *Annual Review of Fluid Mechanics*, Vol. 44, 2012, pp. 527–561.

[3]Fedorov, A., "Transition and Stability of High-Speed Boundary Layers," *Annual Review of Fluid Mechanics*, Vol. 43, 2011, pp. 79–95.

[4]Mack, L. M., "Boundary Layer Linear Stability Theory," Tech. rep., AGARD report No. 709, 1984.

[5]Gushchin, V. and Fedorov, A., "ASYMPTOTIC ANALYSIS OF INVISCID PERTURBATIONS IN A SUPERSONIC BOUNDARY LAYER," *Journal of Applied Mechanics and Technical Physics*, Vol. 30, No. 1, 1989, pp. 64–70.

[6]Demetriades., A., "Hypersonic viscous flow over a slender cone; part iii: Laminar instability and transition." *AIAA*

74-535, 1974.

[7]Zhang, C.-H., Tang, Q., and Lee, C.-B., "Hypersonic boundary-layer transition on a flared cone," *Acta Mechanica Sinica*, Vol. 29, No. 1, 2013, pp. 48–53.

[8]Zhong, X. and Ma, Y., "Boundary-layer receptivity of Mach 7.99 flow over a blunt cone to free-stream acoustic waves," *Journal of Fluid Mechanics*, Vol. 556, 2006, pp. 55–103.

[9]Parsons, N., Zhong, X., Kim, J., and Eldredge, J., "Numerical Study of Hypersonic Receptivity with Thermochemical Non-Equilibrium on a Blunt Cone," *AIAA 2010-4446*, 2010.

[10]Heitmann, D. and Radespiel, R., "Simulation of the interaction of a laser generated shock wave with a hypersonic conical boundary layer," *AIAA 2011-3875*, 2011.

[11]Mack, L., "Review of Linear Compressible Stability Theory," *Stability of Time Dependent and Spatially Varying Flows*, edited by D. Dwoyer and M. Hussaini, Springer-Verlag, 1985, pp. 164–187.

[12]Mack, L. M., "On the Inviscid Acoustic-Mode Instability of Supersonic Shear Flows Part 1: Two-Dimensional Waves," *Theoretical Computational Fluid Dynamics*, Vol. 2, 1990, pp. 97–123.

[13]Chang, C.-L., Vinh, H., and Malik, M., "Hypersonic Boundary-Layer Stability with Chemical Reactions using PSE," *28th AIAA Fluid Dynamics Conference, Snowmass Village, CO, U.S.A.*, 1997.

[14]Salemi, L., *Numerical Investigation of Hypersonic Conical Boundary-Layer Stability Including High-Enthalpy and Three-Dimensional Effects*, Ph.D. thesis, University of Arizona, 2016.

[15]Fedorov, A., Bres, G., Inkman, M., and Colonius, T., "Instability of hypersonic boundary layer on a wall with resonating micro-cavities," *49th AIAA Aerospace Sciences Meeting*, , No. AIAA 2011-373, 2011.

[16]Wagnild, R., *High Enthalpy Effects on Two Boundary Layer Disturbances in Supersonic and Hypersonic Flow*, Ph.D. thesis, University of Minnesota, 240 Williamson Hall, 231 Pillsbury Drive S.E., Minneapolis, MN 55455, May 2012.

[17]Bres, G., Inkman, M., Colonius, T., and Fedorov, A., "Second-mode attenuation and cancellation by porous coatings in a high-speed boundary layer," *Journal of Fluid Mechanics*, Vol. 726, 2013, pp. 312–337.

[18]Klentzman, J. and Tumin, A., "Stability and receptivity of high speed boundary layers in oxygen," *AIAA 2013-2882*, 2013.

[19]Jewell, J., *Boundary-Layer Transition on a Slender Cone in Hypervelocity Flow with Real Gas Effects*, Ph.D. thesis, California Institute of Technology, 2014.

[20]Fedorov, A., Soudakov, V., and Leyva, I., "Stability analysis of high-speed boundary-layer flow with gas injection," *7th AIAA Theoretical Fluid Mechanics Conference*, , No. AIAA 2014-2498, 2014.

[21]Sescu, A., Sawaya, J., Sassanis, V., and Visbal, M., "Study of the Effect of Two-dimensional Wall Non-uniformities on High-speed Boundary Layers," *AIAA 2017-4511*, 2017.

[22]Bitter, N. and Shepherd, J., "Stability of highly cooled hypervelocity boundary layers," *Journal of Fluid Mechanics*, Vol. 778, 2015, pp. 586–620.

[23]Chuvakhov, P. and Fedorov, A., "Spontaneous radiation of sound by instability of a highly cooled hypersonic boundary layer," *8th AIAA Flow Control Conference*, , No. AIAA 2016-4245, 2016.

[24]Edwards, L. and Tumin, A., "Real Gas Effects on Receptivity to Kinetic Fluctuations: I. Mean Flow Effect," *AIAA 2017-0070*, 2017.

[25]Knisely, C. and Zhong, X., "Supersonic Modes in Hot-Wall Hypersonic Boundary Layers with Thermochemical Nonequilibrium Effects," *AIAA 2018-2085*, 2018.

[26]Knisely, C. and Zhong, X., "The Supersonic Mode and the Role of Wall Temperature in Hypersonic Boundary Layers with Thermochemical Nonequilibrium Effects," *AIAA Paper 2018-3218*, June 2018.

[27]Mortensen, C. H., "Toward an understanding of supersonic modes in boundary-layer transition for hypersonic flow over blunt cones," *Journal of Fluid Mechanics*, Vol. 846, 2018, pp. 789–814.

[28]Stuckert, G. and Reed, H., "Linear Disturbances in Hypersonic, Chemically Reacting Shock Layers," *AIAA Journal*, Vol. 32, No. 7, 1994, pp. 1384–1393.

[29]Hudson, M. L., Chokani, N., and Candler, G., "Linear Stability of Hypersonic Flow in Thermochemical Nonequilibrium," *AIAA Journal*, Vol. 35, No. 6, 1997, pp. 958–964.

[30]Johnson, H. B., Seipp, T. G., and Candler, G., "Numerical study of hypersonic reacting boundary layer transition on cones," *Physics of Fluids*, Vol. 10, No. 10, 1998, pp. 2676–2685.

[31]Johnson, H. B. and Candler, G., "Hypersonic Boundary Layer Stability Analysis Using PSE-Chem," *AIAA 2005-5023*, 2005.

[32]Johnson, H. B. and Candler, G., "Analysis of Laminar-Turbulent Transition in Hypersonic Flight Using PSE-Chem," *AIAA 2006-3057*, 2006.

[33]Knisely, C. and Zhong, X., "An Investigation of Sound Radiation by Supersonic Unstable Modes in Hypersonic Boundary Layers," *AIAA 2017-4516*, 2017.

[34]Mortensen, C. H. and Zhong, X., "High-Order Shock-Fitting Method for Hypersonic Flow with Graphite Ablation and Boundary Layer Stability," *AIAA 2012-3150*, 2012.

[35]Mortensen, C. H. and Zhong, X., "Numerical Simulation of Graphite Ablation Induced Outgassing Effects on Hypersonic Boundary Layer Receptivity over a Cone Frustum," *AIAA 2013-0522*, 2013.

[36]Mortensen, C. H. and Zhong, X., "Real Gas and Surface Ablation Effects on Hypersonic Boundary Layer Instability over a Blunt Cone," *AIAA 2013-2981*, 2013.

[37]Mortensen, C. H. and Zhong, X., "Simulation of Second-Mode Instability in a Real-Gas Hypersonic Flow with Graphite Ablation," *AIAA Journal*, Vol. 52, No. 8, 2014, pp. 1632–1652.

[38]Mortensen, C. H. and Zhong, X., "Numerical Simulation of Hypersonic Boundary-Layer Instability in a Real Gas with Two-Dimensional Surface Roughness," *AIAA 2015-3077*, 2015.

[39]Mortensen, C. H., *Effects of Thermochemical Nonequilibrium on Hypersonic Boundary-Layer Instability in the Presence of Surface Ablation and Isolated Two-Dimensional Roughness*, Ph.D. thesis, University of California Los Angeles, 2015.

[40]Zhong, X., "High-Order Finite-Difference Schemes for Numerical Simulation of Hypersonic Boundary-Layer Transition," *Journal of Computational Physics*, Vol. 144, No. 2, 1998, pp. 662–709.

[41]Liu, Y. and Vinokur, M., "Nonequilibrium Flow Computations. I. An Analysis of Numerical Formulations of Conservation Laws," *Journal of Computational Physics*, Vol. 83, No. 2, 1989, pp. 373–397.

[42]Prakash, A., Parsons, N., Wang, X., and Zhong, X., "High-order Shock-fitting Methods for Direct Numerical Simulation of Hypersonic Flow with Chemical and Thermal Nonequilibrium," *Journal of Computational Physics*, Vol. 230, No. 23, 2011, pp. 8474–8507.

[43]Williamson, J., "Low-Storage Runge-Kutta Schemes," *Journal of Computational Physics*, Vol. 35, No. 1, 1980, pp. 48–56.

[44]Malik, M. R., "Numerical Methods for Hypersonic Boundary Layer Stability," *Journal of Computational Physics*, Vol. 86, 1990, pp. 376–413.

[45]Ma, Y. and Zhong, X., "Receptivity of a supersonic boundary layer over a flat plate. Part 1. Wave structures and interactions," *Journal of Fluid Mechanics*, Vol. 488, 2003, pp. 31–78.

[46]Ma, Y. and Zhong, X., "Receptivity of a supersonic boundary layer over a flat plate. Part 2. Receptivity to free-stream sound," *Journal of Fluid Mechanics*, Vol. 488, 2003, pp. 79–121.

[47]Ma, Y. and Zhong, X., "Receptivity of a supersonic boundary layer over a flat plate. Part 3. Effects of different types of free-stream disturbances," *Journal of Fluid Mechanics*, Vol. 532, 2003, pp. 63–109.

[48]Anderson, E., Bai, Z., Bischof, C., Blackford, S., Demmel, J., garra, J. D., Croz, J. D., Greenbaum, A., Hammarling, S., McKenney, A., and Sorensen., D., *LAPACK Users' Guide*, Society for Industrial and Applied Mathematics, Philadelphia, PA, 3rd ed., 1999.